Environmental Science & Technology

Article

Cite This: Environ. Sci. Technol. 2019, 53, 4892−4900

pubs.acs.org/est

Nitrite-Induced Activation of Iodate into Molecular Iodine in Frozen Solution

Kitae Kim,[†,‡] Jinjung Ju,[§] Bomi Kim,[†,‡] Hyun Young Chung,[†,‡] L'ubica Vetráková,[∥] Dominik Heger,[∥] Alfonso Saiz-Lopez,[⊥] Wonyong Choi,[#] and Jungwon Kim*[,§]

[†]Korea Polar Research Institute (KOPRI), Incheon 21990, Republic of Korea

[‡]Department of Polar Sciences, University of Science and Technology (UST), Incheon 21990, Republic of Korea

[§]Department of Environmental Sciences and Biotechnology, Hallym University, Chuncheon, Gangwon-do 24252, Republic of Korea

[∥]Department of Chemistry and Research Centre for Toxic Compounds in the Environment (RECETOX), Faculty of Science, Masaryk University, Kamenice 5, 625 00 Brno, Czech Republic

[⊥]Department of Atmospheric Chemistry and Climate, Institute of Physical Chemistry Rocasolano, CSIC, Madrid 28006, Spain

[#]Division of Environmental Science and Engineering, Pohang University of Science and Technology (POSTECH), Pohang 37673, Republic of Korea

Supporting Information

ABSTRACT: A new mechanism for the abiotic production of molecular iodine (I_2) from iodate (IO_3^-), which is the most abundant iodine species, in dark conditions was identified and investigated. The production of I_2 in aqueous solution containing IO_3^- and nitrite (NO_2^-) at 25 °C was negligible. However, the redox chemical reaction between IO_3^- and NO_2^- rapidly proceeded in frozen solution at −20 °C, which resulted in the production of I_2, I^-, and NO_3^-. The rapid redox chemical reaction between IO_3^- and NO_2^- in frozen solution is ascribed to the accumulation of IO_3^-, NO_2^-, and protons in the liquid regions between ice crystals during freezing (freeze concentration effect). This freeze concentration effect was verified by confocal Raman microscopy for the solute concentration and UV−visible absorption spectroscopy with cresol red (acid−base indicator) for the proton concentration. The freezing-induced production of I_2 in the presence of IO_3^- and NO_2^- was observed under various conditions, which suggests this abiotic process for I_2 production is not restricted to a specific region and occurs in many cold regions. NO_2^--induced activation of IO_3^- to I_2 in frozen solution may help explain why the measured values of iodine are larger than the modeled values in some polar areas.

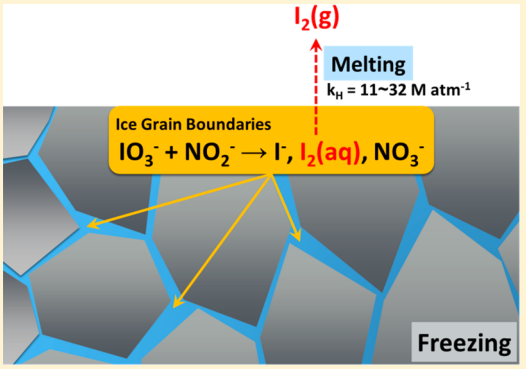

INTRODUCTION

Reactive iodine species, such as atomic iodine(I), molecular iodine (I_2), iodine monoxide (IO), iodine dioxide (OIO), and hypoiodous acid (HOI), play important roles in the tropospheric ozone (O_3) depletion and atmospheric new particle formation in the polar regions.[1] I atoms rapidly react with O_3 to form IO ($I + O_3 \rightarrow IO + O_2$), OIO ($IO + IO \rightarrow I + OIO$), and HOI ($IO + HO_2 \rightarrow HOI + O_2$), which also initiate various tropospheric O_3 depletion cycles.[2−4] In addition, IO and OIO induce the formation of iodine oxides (e.g., I_2O_3, I_2O_4, and I_2O_5) that polymerize to form iodine oxide particles (diameter = 3−10 nm), which serve as a cloud condensation nuclei.[5−7]

The major origin of atmospheric I atoms is the photolysis of organic iodine (e.g., CH_3I and CH_2I_2) and I_2 biologically generated from marine algae (e.g., seaweeds, phytoplankton, and polar microalgae) ($CH_3I + h\nu \rightarrow CH_3 + I$ and $I_2 + h\nu \rightarrow 2I$).[1] Organic iodine is produced mainly by marine algae containing I^- and organic matters through the enzyme-induced methylation of I^- and enzyme/H_2O_2-mediated oxidation of I^-.[8,9] The oxidation of I^- by hydrogen peroxide (H_2O_2) in the cell apoplast of algae produces I_2 through the formation of HOI ($I^- + H_2O_2 \rightarrow HOI + OH^-$; $HOI + I^- + H^+ \rightarrow I_2 + H_2O$).[10,11] Although biological processes are regarded as the main route for the production of organic iodine and I_2,[12,13] abiotic production routes are also required to explain the total atmospheric iodine budget. A few studies have suggested abiotic mechanisms for the production of organic iodine and I_2. For example, I_2 can be produced on the ocean surface through photochemical ($4I^- + O_2 + 2H_2O + h\nu \rightarrow 2I_2 + 4OH^-$)[14] and chemical reactions ($I^- + O_3 + H^+ \rightarrow HOI + O_2$; $HOI + I^- + H^+ \rightarrow I_2 + H_2O$).[15,16] In addition, reactions between methyl radicals (generated from the photolysis of humic substances) and I atoms (generated from the oxidation

Received: November 24, 2018
Revised: March 8, 2019
Accepted: March 27, 2019
Published: March 27, 2019

DOI: 10.1021/acs.est.8b06638
Environ. Sci. Technol. 2019, 53, 4892−4900

of I^- by photochemically generated oxidants)[17] and between I_2/HOI (generated from chemical and photochemical reactions) and dissolved organic matter[18] contribute to the formation of organic iodine. However, abiotic routes for the production of organic iodine and I_2 have been much less investigated than biogenic production routes and are largely unknown at this stage.

The freezing point of aqueous solution is the temperature at which the conversion of liquid water to ice crystals starts and the term "frozen solution" in this study refers to the solution containing both liquid regions and ice crystals. At temperatures below the eutectic point, the liquid regions between ice crystals completely disappear. In general, redox chemical reactions in frozen solutions (i.e., at temperatures below the freezing point) are slower than those in aqueous solutions (i.e., at temperatures above the freezing point). However, redox chemical reactions between specific reactants (e.g., NO_2^-/O_2, chromate ($HCrO_4^-$)/H_2O_2, $NO_2^-/HCrO_4^-$, bromate (BrO_3^-)/humic substance, and periodate (IO_4^-)/furfuryl alcohol) proceed more rapidly in frozen solutions.[19−23] Frozen solutions at temperatures between the freezing and eutectic points contain a liquid phase between solid ice crystals, the so-called liquid brine, ice grain boundary, or micropocket.[24,25] As ice crystals grow, solutes and dissolved gases are gradually accumulated in the liquid regions surrounded by ice crystals,[26,27] which act as microsized reactors. In addition, the exclusion of protons (or hydroxides) from ice crystals to the liquid regions changes the pH of the reaction site (i.e., liquid regions between ice crystals) and the speciation of reactants.[28] The concentration of solutes, dissolved gases, and protons (or hydroxides) by freezing (i.e., freeze concentration effect) is regarded as the main reason for the faster redox chemical reactions in frozen solutions.

Recently, the role of ice media on the abiotic production of I_2 has been introduced. The redox chemical reaction between I^- and NO_2^-, which is negligible in aqueous solution, proceeds in frozen solution to generate I_2 (or tri-iodide, I_3^-) and NO_3^- (or nitric oxide, NO).[29−31] The pH decrease by freezing converts NO_2^- to the nitroacidium ion (H_2ONO^+) and nitrous acid (HONO), which can oxidize I^- to I_2 ($2H_2ONO^+ + 2I^- \rightarrow I_2 + 2NO + 2H_2O$ and $HONO + 2I^- + O_2 + H^+ \rightarrow I_2 + NO_3^- + H_2O$). The photochemical production of I_2 and I_3^- in the presence of I^- is markedly enhanced when aqueous solutions of I^- are frozen.[32,33] The concentration of I^- and O_2 in the liquid regions between ice crystals by freezing induces the formation of an $I^-\cdot O_2$ complex. UV irradiation ($\lambda > 300$ nm) of the $I^-\cdot O_2$ complex enables the electron transfer from I^- to O_2 (inner sphere electron transfer) to generate I atoms as precursors of I_2 and I_3^- ($I^-\cdot O_2 + h\nu \rightarrow I + O_2^-$). It has been also reported that I_2 and other reactive iodine species, such as IO and OIO, can be produced from the photolysis of the frozen solution of IO_3^- and the frozen NH_4IO_3 salt.[34,35] However, a mechanism for this has not been proposed.

The mechanism of organic iodine and I_2 production through biological, chemical, and photochemical processes has been extensively investigated. However, most studies have focused on the conversion of I^- rather than IO_3^- to organic iodine or I_2. Iodine species are mainly found as I^- and IO_3^- in snow, sea ice, seawater, surface water, and atmospheric aerosols. Between these two iodine species, IO_3^- is more abundant.[36,37] NO_2^- is one of the major inorganic nitrogen species in natural waters and rainwater.[38,39] NO_2^- is naturally generated by the oxidation of NH_4^+ by *Nitrosomonas europaea* (nitrifying bacteria) and the decomposition of copepod feces and algae in the presence of *Nitrosocystis oceanus* (nitrifying bacteria).[40,41] Various industries, such as food preservation, fertilizer manufacturing, and corrosion inhibition, use chemical reagents containing high concentrations of NO_2^-.[42] The agricultural application of fertilizers also contributes to the increase in NO_2^- levels in water and soil.[43]

Herein, we report a new mechanism for the production of I_2 from IO_3^-, that is, the abiotic production of I_2 in the frozen solution containing IO_3^- and NO_2^- in the dark. The freezing-induced production of I_2 was measured as a function of various experimental parameters, such as pH, IO_3^- and NO_2^- concentrations, and freezing temperature. Furthermore, the mechanism of I_2 production is proposed based on a variety of experimental evidence.

EXPERIMENTAL SECTION

Chemicals. The following chemicals were used as received without further purification: potassium iodate (KIO_3, Sigma-Aldrich, ≥ 99.5%), potassium iodide (KI, Junsei, ≥ 99.5%), sodium nitrite ($NaNO_2$, Sigma-Aldrich, ≥ 99.0%), sodium nitrate ($NaNO_3$, Sigma-Aldrich, ≥ 99.0%), cresol red ($C_{21}H_{18}O_5S$, Sigma-Aldrich, ≥ 95.0%), sodium carbonate (Na_2CO_3, Sigma-Aldrich, ≥ 99.5%), and sodium bicarbonate ($NaHCO_3$, Sigma-Aldrich, ≥ 99.7%). All solutions were prepared with ultrapure deionized water (resistivity ≥18.2 MΩ·cm), which was obtained from a Human-Power I+ water purification system (Human Corporation).

Experimental Procedure. Aliquots of IO_3^- and NO_2^- stock solutions were added to deionized water in a beaker to yield the desired initial concentration (usually $[IO_3^-] = 1$ mM and $[NO_2^-] = 1$ mM). The solution pH was adjusted using a $HClO_4$ or NaOH solution to the desired value (usually pH 3.0). Then, 10 mL of this solution was put in a 15 mL polypropylene conical tube that was sealed with a cap. The solution was unbuffered and air-equilibrated. The conical tube containing the aqueous solution of IO_3^- and NO_2^- was placed in a conical tube rack in a cooling bath, which was precooled to the desired temperature (usually −20 °C), to freeze the aqueous solution. Ethanol was used as the coolant. The term "freezing temperature" in this study refers to the temperature of ethanol in the cooling bath. The moment at which the conical tube containing the aqueous solution was introduced into the cooling bath was taken as the reaction starting point (reaction/freezing time = 0 h). The conical tube containing the frozen solution was withdrawn from the cooling bath and then put into lukewarm water bath at 35 °C to thaw the frozen sample for chemical analyses. After thawing, the aqueous sample was immediately analyzed. The experiments in a cooling bath preset at 25 °C were also performed to investigate chemical reactions in aqueous solution as control tests. Multiple experiments were performed for a given set of conditions to confirm the reproducibility of the data.

Chemical Analyses. The quantitative analyses of anions, such as I^-, IO_3^-, NO_2^-, and NO_3^-, were performed using an ion chromatograph (Dionex ICS-1100) equipped with a Dionex IonPac AG14 guard column (4 mm × 50 mm), a Dionex IonPac AS14 column (4 mm × 250 mm), and a conductivity detector. The eluent was a binary mixture of Na_2CO_3 (3.5 mM) and $NaHCO_3$ (1 mM), and its flow rate was 1.0 mL/min. The concentration of I_2 was determined by measuring the absorbance of the aqueous sample at 460 nm (ε = 746 M^{-1} cm^{-1})[44] using a UV−visible spectrophotometer (Shimadzu UV-2600).

DOI: 10.1021/acs.est.8b06638
Environ. Sci. Technol. 2019, 53, 4892−4900

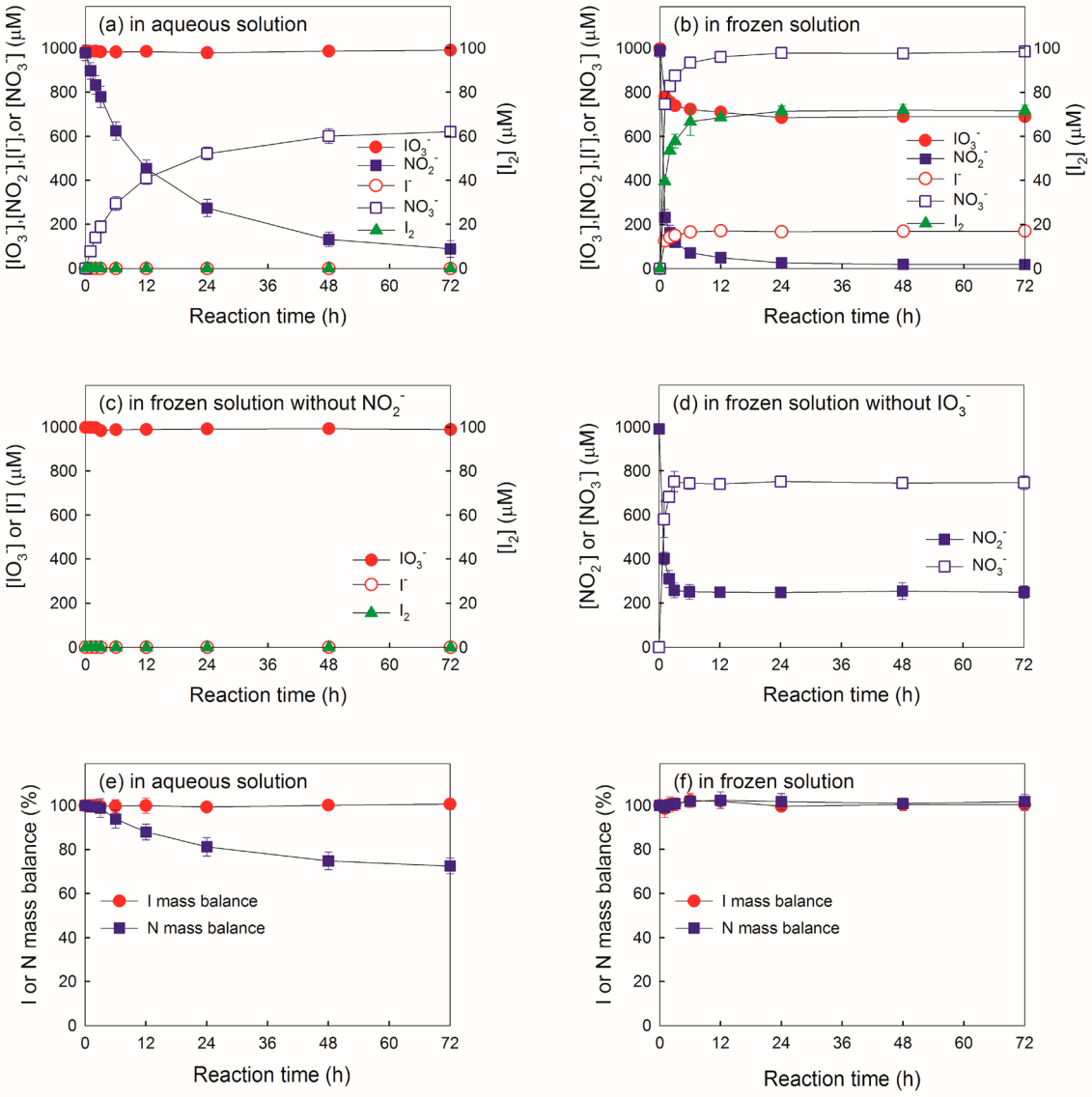

Figure 1. Time profiles of the concentrations of IO_3^-, NO_2^-, I_2, I^-, and NO_3^- in (a) aqueous and (b) frozen solutions containing IO_3^- and NO_2^-. (c) Production of I_2 and I^- in the frozen solution of IO_3^-. (d) Production of NO_3^- in the frozen solution of NO_2^-. Nitrogen and iodine mass balances in (e) aqueous and (f) frozen solutions containing IO_3^- and NO_2^-. Experimental conditions: $[NO_2^-]$ = 1 mM, $[IO_3^-]$ = 1 mM, pH 3.0, aqueous solution temperature = 25 °C, and freezing temperature = −20 °C.

Estimation of the pH of the Frozen Solution. The pH of the frozen solution was estimated by measuring the UV−visible absorption spectra of cresol red (CR) as an acid−base indicator after freezing but without thawing.[45,46] The relative concentrations of two different CR species ([singly protonated CR]/[doubly protonated CR] or [deprotonated CR]/[singly protonated CR]) were obtained from the UV−visible absorption spectra of CR by non-negative least-squares minimization (eq 1). Then, the pH of the frozen solution was calculated using the simple relationship between the relative concentrations of two different CR species, pK_a, and pH (eq 2) (see Discussion of pH estimation in the Supporting Information (SI) for details).

$$\sum_{\lambda=400\text{nm}}^{650\text{nm}} (A\cdot a + B\cdot b - X)^2 = \text{minimum value} \quad (1)$$

Here, X is the absorbance of frozen solution, A and B are the absorbances of two different CR species, and a and b are the relative concentrations of two different CR species, respectively.

$$\text{pH} = \text{p}K_{a1} + \log\frac{[\text{singly protonated CR}]}{[\text{doubly protonated CR}]} \left(\text{or } \text{p}K_{a2} + \log\frac{[\text{deprotonated CR}]}{[\text{singly protonated CR}]}\right) \quad (2)$$

Measurement of IO_3^- Distribution in Frozen Solution. The distribution of IO_3^- in frozen solution was investigated using confocal Raman microscope (Renishaw inVia). 100 μL of IO_3^- solution ($[IO_3^-]$ = 1 mM and pH 3.0) was dropped on the cover glass on the temperature controlled stage (Linkam scientific THMS600) at lowest temperature = −20 °C. A monochromatic laser with a wavelength of 532 nm was used as

DOI: 10.1021/acs.est.8b06638
Environ. Sci. Technol. 2019, 53, 4892−4900

the excitation source, and chemical mapping image was obtained by measuring the peak intensity at 942 cm^{-1}.

RESULTS AND DISCUSSION

Generation of I_2 by Freezing in the Presence of IO_3^- and NO_2^-. The redox chemical reaction between IO_3^- and NO_2^- in frozen solution at −20 °C was investigated and compared with that in aqueous solution at 25 °C (Figure 1). The concentration of NO_2^- gradually decreased with reaction time with the generation of NO_3^- in aqueous solution, whereas the conversion of IO_3^- was negligible during the whole reaction time (Figure 1a). This result indicates that the redox conversion of IO_3^- and NO_2^- does not occur in aqueous solution. Under this situation, the oxidation of NO_2^- to NO_3^- should be attributed to the reaction of NO_2^- with O_2 or H^+ ($2NO_2^- + O_2 \rightarrow 2NO_3^-$, $3NO_2^- + 2H^+ \rightarrow NO_3^- + 2NO + H_2O$, or $4NO_2^- + 2H^+ \rightarrow N_2O + 2NO_3^- + H_2O$).[47,48] The generation of NO_3^- in aqueous solution of IO_3^- and NO_2^- was markedly retarded when the solution was purged with Ar gas to remove dissolved oxygen (see SI Figure S1). This result indicates that the reaction of NO_2^- with O_2 is more favored than that with H^+. In contrast to the aqueous-phase reaction, the concentrations of both IO_3^- and NO_2^- decreased and, at the same time, the concentrations of I^-, I_2, and NO_3^- increased in frozen solution (Figure 1b). The production of I_2 and I^- was initiated after 10 min at which the liquid and solid phases coexisted (see SI Figure S2). The aqueous solution containing IO_3^- and NO_2^- was "apparently" completely frozen after 30 min (see SI Figure S3). However, the liquid regions between ice crystals must have existed longer because the production of I_2 and I^- was observed after 30 min. After 24 h of freezing reaction, 72 (±2) μM of I_2 and 167 (±2) μM of I^- were generated from the reduction of 314 (±1) μM of IO_3^-. At the same time, 961 (±18) μM of NO_2^- was oxidized and 978 (±7) μM of NO_3^- was generated. However, the concentration of IO_3^- in frozen solution was not changed in the absence of NO_2^- (Figure 1c). Therefore, the production of I^-, I_2 (reduction products of IO_3^-), and NO_3^- (oxidation product of NO_2^-) in the frozen solution containing IO_3^- and NO_2^- implies that the redox conversion of IO_3^- and NO_2^- is favored in frozen solution (reactions 3 and 4).

$$IO_3^- + 3HNO_2 \rightarrow I^- + 3NO_3^- + 3H^+,\ E^0 = 0.151V_{NHE} \quad (3)$$

$$2IO_3^- + 5HNO_2 \rightarrow I_2 + 5NO_3^- + 3H^+ + H_2O,\ E^0 = 0.261V_{NHE} \quad (4)$$

Here, E^0 was obtained by combining the half-reduction reactions of IO_3^- to I^- (E^0 = 1.085 V_{NHE}), IO_3^- to I_2 (E^0 = 1.195 V_{NHE}), and NO_3^- to HNO_2 (E^0 = 0.934 V_{NHE}).[49]

The production of I_2 and I^- through the NO_2^--mediated reduction of IO_3^- proceeded only while NO_2^- was oxidized to NO_3^- (i.e., for 24 h). When the oxidation of NO_2^- was complete, the generation of I_2 and I^- stopped, despite the presence of residual IO_3^-. This behavior implies that only NO_2^- acts as a reductant for the conversion of IO_3^- to I^- and I_2. The oxidation of NO_2^- to NO_3^- in the frozen solution of NO_2^- (i.e., in the absence of IO_3^-) was observed, and its rate was much higher than that in the aqueous solution (Figure 1d). The enhanced oxidation of NO_2^- in the frozen solution is due to the accumulation of O_2 in the liquid regions between ice crystals during freezing, which enhances the reaction between NO_2^- and O_2.[20] However, the observed molar ratio of oxidized NO_2^- to reduced IO_3^- in the frozen solution containing IO_3^- and NO_2^- was 3.1 (Figure 1b), which is similar to the theoretical (stoichiometric) value (2.5−3.0) according to reactions 3 and 4. This result indicates that the oxidation of NO_2^- by IO_3^- is more favored than that by O_2 in frozen solution.

Figures 1e and f show the iodine ((($[IO_3^-]$ + $[I^-]$ + 2 × $[I_2]$)/initial $[IO_3^-]$ × 100) and nitrogen mass balances (($[NO_2^-]$ + $[NO_3^-]$)/initial $[NO_2^-]$ × 100) in aqueous and frozen solutions containing IO_3^- and NO_2^-, respectively. Because IO_3^- is inert to NO_2^- in aqueous solution, 100% iodine mass balance was achieved in aqueous solution. However, the nitrogen mass deficits were over 25% after 48 h of reaction. The incomplete nitrogen mass balance is most likely due to both the emission of HNO_2 to the atmosphere in a gaseous form (Henry's law constant of HNO_2 for water as solvent = 37.5−48.6 M atm^{-1})[50] and the conversion of NO_2^- to other nitrogen species such as nitrogen monoxide (NO) and nitrous oxide (N_2O)[48] (see SI Figure S1 and accompanying discussion in the SI for details). On the other hand, both iodine and nitrogen mass balances were satisfactory in frozen solution, which confirms that reactions 3 and 4 are the dominant redox chemical reactions between IO_3^- and NO_2^- in frozen solution and other side reactions are negligible.

SI Figure S4a shows the images of the samples containing IO_3^- and NO_2^- as a function of freezing time. The color of I_2 depends on the type of solvent due to different I_2-solvent interactions (e.g., brown in water and ethanol and violet in carbon tetrachloride and chloroform).[51] The samples gradually turned yellowish-brown with freezing time. These images directly illustrate the production of I_2 in the frozen solution containing IO_3^- and NO_2^-. In accordance with the color change by freezing, the absorbance at 460 nm, which is ascribed to the generation of I_2,[44] gradually increased with freezing time (SI Figure S4b).

When the frozen solution was thawed and then kept in the dark under ambient conditions, the absorbance at 460 nm gradually decreased as time went on (SI Figure S5). This result indicates that I_2 trapped in the frozen solution is slowly emitted to the atmosphere after melting (Henry's law constant of I_2 for water as solvent = 11.1−32.4 M atm^{-1}),[50] which may contribute to the significant iodine concentration and ozone depletion in the polar regions during springtime.[52,53]

Mechanism of I_2 Production. It has been reported that the concentration of protons increases when the acidic aqueous solution is frozen due to the freeze concentration effect.[28] The degree of pH decrease by freezing depends on various parameters such as freezing temperature and rate, solute type and concentration, and solvent type. To investigate how much the pH decreases by freezing in our system (i.e., at $[NO_2^-]$ = 1 mM, $[IO_3^-]$ = 1 mM, pH 3.0 in aqueous solution, and freezing temperature = −20 °C), the UV−visible absorption spectra of the frozen solution containing IO_3^-, NO_2^-, and CR were measured without thawing (Figure 2). Only one peak at 434 nm was observed in aqueous solution at pH 3.0. This result is consistent with the fact that about 99% of CR species exist as singly protonated CR (λ_{max} = 434 nm)[54] at pH 3.0 (see SI Figure S6). When the aqueous solution containing IO_3^- and NO_2^- at pH 3.0 was frozen, the peak at 434 nm decreased and the peak at 518 nm increased. This result indicates that some singly protonated CR was changed to doubly protonated CR (λ_{max} = 518 nm)[54] (i.e., the pH decreased) after freezing. The ratio of [singly protonated CR] to [doubly protonated CR] in frozen solution was calculated

DOI: 10.1021/acs.est.8b06638
Environ. Sci. Technol. 2019, 53, 4892−4900

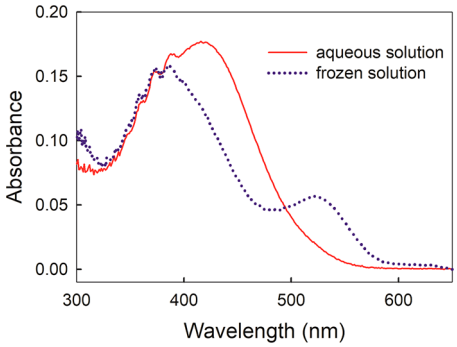

Figure 2. UV−visible absorption spectra of CR in aqueous and frozen solutions containing IO_3^-, NO_2^-, and CR. Experimental conditions: $[NO_2^-]$ = 1 mM, $[IO_3^-]$ = 1 mM, [CR] = 50 μM, pH 3.0, aqueous solution temperature = 25 °C, and freezing temperature = −20 °C.

by fitting the data in Figure 2 to eq 1 and was estimated to be approximately 5:1. Therefore, the pH of the frozen solution with $[NO_2^-]$ = 1 mM, $[IO_3^-]$ = 1 mM, pH 3.0 in aqueous solution, and freezing temperature = −20 °C was 1.8. This value was obtained by inserting the [singly protonated CR]/[doubly protonated CR] value (5.00) and pK_{a1} value of CR (1.10)[55,56] into eq 2 (see SI Figure S6).

In the aqueous solution containing IO_3^- (pK_a = 0.78)[57] and NO_2^- (pK_{a1} = 1.7 and pK_{a2} = 2.8)[58] at pH 3.0, IO_3^- is the dominant form (99.4%), and NO_2^- mainly exists as NO_2^- (60.2%) and HONO (38.0%). When the aqueous solution containing IO_3^- and NO_2^- at pH 3.0 is frozen (i.e., when the pH decreases to 1.8), the molar fractions of IO_3^- and NO_2^- species become as follows: 91.3% for IO_3^-, 8.7% for HIO_3, 5.3% for NO_2^-, 52.8% for HONO, and 41.9% for H_2ONO^+ (SI Figure S7). The most striking difference of IO_3^- and NO_2^- speciation between aqueous solution and frozen solution is the existence of H_2ONO^+. The concentration of H_2ONO^+ is negligible in aqueous solution at pH 3.0 but significant in the frozen solution due to the pH decrease to 1.8. It is well-known that H_2ONO^+ is much more reactive than HONO and NO_2^-.[59,60] Therefore, the production of I_2 through the redox chemical reaction between IO_3^- and NO_2^- in frozen solution is most likely due to the generation of H_2ONO^+ by the freezing-induced pH decrease.

Although the reduction of IO_3^- by HONO is thermodynamically possible according to reactions 3 and 4, the negligible conversion of IO_3^- by HONO (38.0%) in aqueous solution at pH 3.0 implies that the redox chemical reaction between IO_3^- and HONO is kinetically very slow. The high reactivity of H_2ONO^+ generated by freezing (by the pH decrease) toward IO_3^- can be ascribed to not only its high reduction power but also the electrostatic attraction between cationic H_2ONO^+ and anionic IO_3^-. The electrostatic attraction between H_2ONO^+ and IO_3^- would facilitate the electron transfer from H_2ONO^+ to IO_3^- by reducing the distance between these species and increasing their collision probability.

The increased concentration of H_2ONO^+ and IO_3^- in the liquid region of frozen solution by exclusion from ice crystals should increase the reaction probability between H_2ONO^+ and IO_3^-, which kinetically accelerates their redox transformation. Figure 3 shows the optical image and IO_3^- distribution of the frozen solution. The pyramidal IO_3^- ions exhibit two strong Raman peaks near 800 cm^{-1} in aqueous solution, which are ascribed to symmetric and antisymmetric stretching of I−O

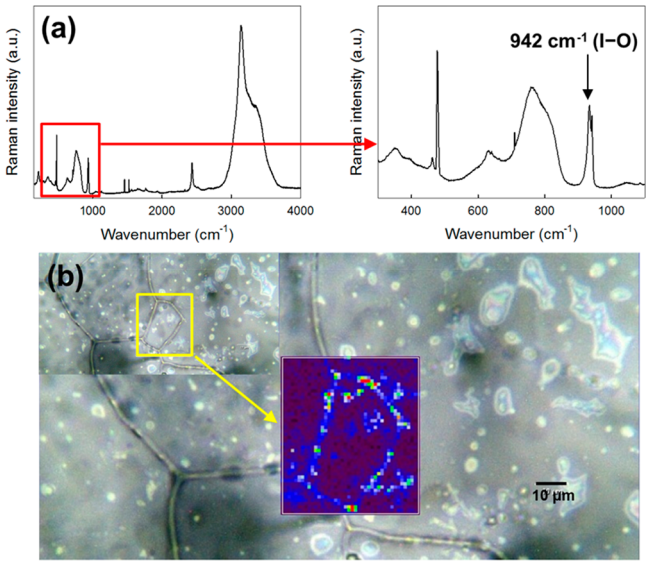

Figure 3. (a) Raman spectra of IO_3^- in frozen solution and (b) optical image of the frozen IO_3^- solution and the distribution of IO_3^- based on the peak intensity at 942 cm^{-1}. Experimental conditions: $[IO_3^-]$ = 1 mM, pH 3.0, and freezing temperature = decrease from 0 °C to −20 °C at a rate of −1.5 °C/min. The concentration of IO_3^- decreases in the order: red, orange, yellow, green, blue, indigo, and violet.

bonds.[61] On the other hand, these two Raman peaks were observed around 900−1000 cm^{-1} in frozen solution (Figure 3a), which indicates that the interaction between IO_3^- and water molecules in frozen solution is different from that in aqueous solution. The IO_3^- mapping image of the frozen IO_3^- solution was obtained based on the peak intensity at 942 cm^{-1}, and its concentrations are represented using a rainbow spectrum (red: high → violet: negligible) (Figure 3b). IO_3^- in frozen solution mainly existed in the liquid regions and IO_3^- trapped in ice crystals was negligible (see SI Figure S8 and accompanying discussion in the SI for details). Overall, freezing induces the formation of H_2ONO^+ from NO_2^- and increases the concentrations of H_2ONO^+ and IO_3^-. These behaviors act synergistically to enhance the production of I_2 in the frozen solution containing IO_3^- and NO_2^-.

To provide convincing evidence for the above hypotheses, we investigated the effect of solute (IO_3^- or NO_2^-) concentration increase and/or pH decrease on the production of I^- and I_2 in aqueous solution (SI Figure S9). The production of both I^- and I_2 in aqueous solution was negligible at $[IO_3^-]$ = 1 mM, $[NO_2^-]$ = 1 mM, and pH 3.0 (reference conditions). An increase in the IO_3^- or NO_2^- concentration by 10 times (1 mM → 10 mM) at pH 3.0 did not induce the formation of I^- and I_2 (SI Figures S9a and b). Despite decreasing the pH to 2.0, where 30% of NO_2^- exists in the H_2ONO^+ form, at $[IO_3^-]$ = 1 mM and $[NO_2^-]$ = 1 mM, the production of both I^- and I_2 was not observed. However, when the concentration of NO_2^- increased to 10 mM and the pH decreased to 2.0, the production of both I^- and I_2 was observed (SI Figures S9c and d). This result clearly indicates that the pH decrease and the solute concentration increase by freeze concentration effect synergistically accelerate the redox chemical reaction between IO_3^- and NO_2^- in frozen solution. In contrast to the case of NO_2^-, the increase in the IO_3^- concentration by 10 times (1 mM → 10 mM) at pH 2.0 did not generate I_2 and I^- above the detection limit (SI Figures

DOI: 10.1021/acs.est.8b06638
Environ. Sci. Technol. 2019, 53, 4892−4900

S9c and d). This result implies that the concentration of NO_2^- (more precisely H_2ONO^+) more significantly affects the redox conversion rate of IO_3^- and NO_2^- (i.e., the production of I_2 and I^-) than the concentration of IO_3^-.

Freezing-Induced Production of I_2 under Various Conditions. The effect of pH, IO_3^- concentration, NO_2^- concentration, and freezing temperature on the production of I_2 and I^- in the frozen solution containing IO_3^- and NO_2^- was investigated (Figure 4). Data collection was performed after 24

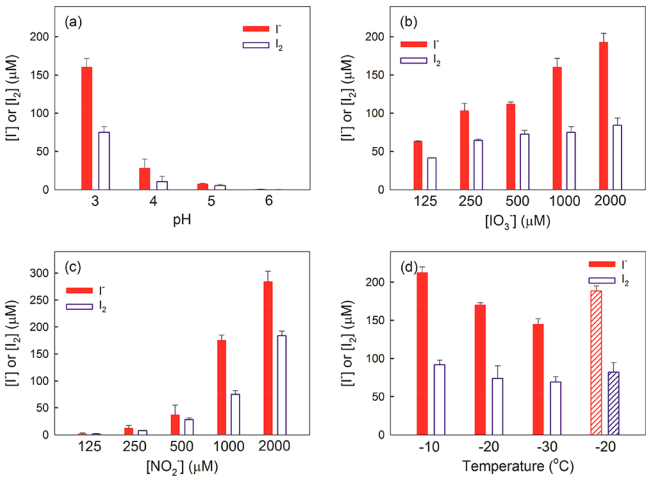

Figure 4. Effect of (a) pH, (b) IO_3^- concentration, (c) NO_2^- concentration, and (d) freezing temperature on the production of I_2 and I^- in the frozen solution containing IO_3^- and NO_2^-. Experimental conditions: $[NO_2^-]$ = 1 mM for parts a, b, and d, $[IO_3^-]$ = 1 mM for parts a, c, and d, pH 3.0 for parts b, c, and d, and freezing temperature = −20 °C for parts a, b, and c. The bars with diagonal stripes correspond to the experiments performed in a refrigerator.

h of reaction because further freezing to 72 h did not produce more I_2 and I^-. The trend for I_2 production agreed with that for I^- production in all cases. Figure 4a shows the production of I_2 and I^- as a function of pH. The production of I_2 and I^- after freezing increased with decreasing pH. This behavior is ascribed to the fact that the pH of the frozen solution is lower and more H_2ONO^+ is produced when an aqueous solution having a lower pH is frozen.

We also investigated the effect of the IO_3^- and NO_2^- concentrations on the production of I_2 and I^-. The production of both I_2 and I^- increased with increasing concentrations of IO_3^- and NO_2^- (Figures 4b and c). Of those of IO_3^- and NO_2^-, the concentration of NO_2^- has greater influence on the production of I_2 and I^-. When the concentration of IO_3^- increased from 125 μM to 2 mM at $[NO_2^-]$ = 1 mM, the production of I_2 doubled (41.4 μM → 84.1 μM). On the other hand, the increase in the NO_2^- concentration from 125 μM to 2 mM at $[IO_3^-]$ = 1 mM resulted in 130-times greater I_2 production (1.4 μM → 183.8 μM). This result reconfirms that the concentration of NO_2^- has a decisive effect on the rate of the redox chemical reaction between IO_3^- and NO_2^-.

We investigated whether the solution containing IO_3^- and NO_2^- ($[NO_2^-]$ = 1 mM, $[IO_3^-]$ = 1 mM, and pH = 3.0) is frozen or not depending on the temperature (−7, − 8, − 9, and −10 °C) (see SI Table S1). According to the results, the freezing point is estimated to be about −8 °C. Figure 4d shows the freezing temperature-dependent production of I_2 and I^-. The production of I_2 and I^- in frozen solutions was observed at all freezing temperatures tested (−10 to −30 °C). However, the amount of I_2 and I^- produced in the frozen solutions varied depending on the freezing temperature. The final production of I_2 and I^- decreased at lower freezing temperatures. After 24 h of reaction, 91.8, 74.1, and 69.2 μM of I_2 (also 212.5, 170.4, and 144.9 μM of I^-) were produced at −10, − 20, and −30 °C, respectively. It has been previously reported that the redox chemical reactions in frozen solution last a shorter time at lower freezing temperature because they are stopped (or markedly retarded) when the liquid region completely disappears on complete solidification (i.e., when there is no liquid region in frozen solution because the temperature of liquid region reaches the eutectic temperature).[20,62−64] The more rapid complete solidification at lower freezing temperature accounts for why the production of I_2 and I^- decreases with decreasing freezing temperature. The production of I_2 and I^- was higher when the solution was frozen in a refrigerator (relatively slow freezing; coolant: cold air) than when frozen in a cooling bath (relatively fast freezing; coolant: cold ethanol) at the same temperature (−20 °C). This result indicates that the freezing rate at the same temperature affects the final production of I_2 and I^-. However, there are other possibilities of the freezing temperature-dependent production of I_2 and I^-. The growth of ice crystals begins earlier at lower freezing temperatures. Therefore, the concentration of solutes in the liquid regions between ice crystals is higher at lower freezing temperatures in the initial period. The production of I_2 and I^- in the initial period (i.e., after 30 min) was in the order −30 > − 20 > − 10 °C (see SI Figure S10). However, slow freezing can eventually accumulate a greater amount of solutes in the liquid regions between ice crystals than fast freezing. The local concentration of methylene blue in the grain boundaries of ice at 243 K was higher by 3 orders of magnitude than that at 77 K.[27] The higher production of I_2 and I^- at higher freezing temperatures may be because IO_3^- and NO_2^- are more concentrated in the grain boundaries of ice under slower freezing conditions. In addition, the rate constant of a chemical reaction based on the Arrhenius equation decreases with decreasing temperature. This may also be the reason for the lower final production of I_2 and I^- at lower freezing temperatures. In real aquatic systems, cold air (not ethanol) acts as the coolant. Therefore, the time that it takes to reach the complete solidification would be longer and the production of I_2 and I^- in the frozen solution containing IO_3^- and NO_2^- would be more significant in real aquatic systems.

Environmental Implications. The production of I_2 through the redox chemical reaction between IO_3^- and NO_2^- in frozen solution may make a significant contribution to the global iodine budget because both IO_3^- and NO_2^- are ubiquitous. The concentrations of NO_2^- and IO_3^- vary significantly depending on region, season, and type of environmental media (e.g., NO_2^-: dozens of nM ∼ a few μM in snow on the Arctic region,[65,66] hundreds of nM ∼ a few μM in seawater,[67,68] and a few μM ∼ hundreds of μM in surface water[69,70] and IO_3^-: dozens of nM ∼ hundreds of nM in sea ice on the Arctic region,[71] hundreds of nM in seawater,[72−74] and dozens of nM ∼ hundreds of nM in surface water[75,76]). Although the concentrations of IO_3^- and NO_2^- in this study are higher than environmentally relevant concentrations, the proposed mechanism can significantly affect the global production of I_2 because it operates in extensive cold regions, such as polar regions, permafrost, and midlatitudes during the winter season.

DOI: 10.1021/acs.est.8b06638
Environ. Sci. Technol. 2019, 53, 4892−4900

Comparing both polar regions, the level of NO_2^- in ice is higher in the Arctic than in the Antarctic due to anthropogenic NO_x (as a precursor of NO_2^-) emissions in the northern hemisphere. In addition, the pH of ice in the Arctic region (4–5) is lower than that in the Antarctic region (4.5–6.5).[77,78] Therefore, the production of I_2 through NO_2^--induced activation of IO_3^- in frozen solution should be higher in the Arctic than in the Antarctic. A recent study reported a rapid increase in atmospheric iodine levels in the Arctic since the midtwentieth century, with potential implications for increased iodine-mediated O_3 depletion in this region in recent decades.[79] Freeze–thaw cycles through day/night temperature variation will produce and emit I_2 in midlatitudes during the winter season. In addition, in permafrost and polar regions, I_2 will be produced and accumulated in ice during the winter season and emitted to the atmosphere in the spring.

No previous mechanisms for the production of organic iodine and I_2 can completely account for the iodine budget in some polar areas, which implies that there is still a missing source and mechanism for organic iodine and/or I_2 production.[35,80] This new mechanism for I_2 production may help explain why the measured values of iodine are larger than the modeled values in some polar areas. The production of I_2 through the redox chemical reaction between IO_3^- and NO_2^- may be low in the polar regions because there are not many sites that meet the specific requirements (i.e., high concentrations of IO_3^- and NO_2^- and low pH). Even then, the freezing-induced production of I_2 from IO_3^- can be initiated by other inorganic and organic species. The redox couple of IO_3^- and NO_2^- is only one example and there would be other species which could reduce IO_3^- to I_2 during freezing. If so, this mechanism has the potential to have more impact on the I_2 emission flux to the atmosphere.

■ ASSOCIATED CONTENT

Supporting Information

The Supporting Information is available free of charge on the ACS Publications website at DOI: 10.1021/acs.est.8b06638.

Discussions of pH estimation, discussions on Figures S1 and S8, supplementary Figures (S1–S10), and Table S1 (PDF)

■ AUTHOR INFORMATION

Corresponding Author

*Phone: +82-33-248-2156; e-mail: jwk@hallym.ac.kr.

ORCID

Kitae Kim: 0000-0003-0803-3547
Dominik Heger: 0000-0002-6881-8699
Wonyong Choi: 0000-0003-1801-9386
Jungwon Kim: 0000-0001-7804-7587

Notes

The authors declare no competing financial interest.

■ ACKNOWLEDGMENTS

This research was supported by the Korea Polar Research Institute (KOPRI) project (PE18200) and Hallym University Research Fund (HRF-201802-012).

■ REFERENCES

(1) Saiz-Lopez, A.; Plane, J. M. C.; Baker, A. R.; Carpenter, L. J.; von Glasow, R.; Martín, J. C. G.; McFiggans, G.; Saunders, R. W. Atmospheric chemistry of iodine. *Chem. Rev.* **2012**, *112*, 1773–1804.

(2) McFiggans, G.; Plane, J. M. C.; Allan, B. J.; Carpenter, L. J.; Coe, H.; O'Dowd, C. A modeling study of iodine chemistry in the marine boundary layer. *J. Geophys. Res.: Atmos.* **2000**, *105*, 14371–14385.

(3) Vogt, R.; Sander, R.; Glasow, R. V.; Crutzen, P. J. Iodine chemistry and its role in halogen activation and ozone loss in the marine boundary layer: a model study. *J. Atmos. Chem.* **1999**, *32*, 375–395.

(4) Saiz-Lopez, A.; Fernandez, R. P.; Ordóñez, C.; Kinnison, D. E.; Martín, J. C. G.; Lamarque, J.-F.; Tilmes, S. Iodine chemistry in the troposphere and its effect on ozone. *Atmos. Chem. Phys.* **2014**, *14*, 13119–13143.

(5) Gálvez, O.; Martín, J. C. G.; Gómez, P. C.; Saiz-Lopez, A.; Pacios, L. F. A theoretical study on the formation of iodine oxide aggregates and monohydrates. *Phys. Chem. Chem. Phys.* **2013**, *15*, 15572–15583.

(6) Saunders, R. W.; Plane, J. M. C. Formation pathways and composition of iodine oxide ultra-fine particles. *Environ. Chem.* **2005**, *2*, 299–303.

(7) Saiz-Lopez, A.; Plane, J. M. C.; McFiggans, G.; Williams, P. I.; Ball, S. M.; Bitter, M.; Jones, R. L.; Hongwei, C.; Hoffmann, T. Modelling molecular iodine emissions in a coastal marine environment: the link to new particle formation. *Atmos. Chem. Phys.* **2006**, *6*, 883–895.

(8) Wuosmaa, A. M.; Hager, L. P. Methyl chloride transferase: a carbocation route for biosynthesis of halometabolites. *Science* **1990**, *249*, 160–162.

(9) Theiler, R.; Cook, J. C.; Hager, L. P.; Siuda, J. F. Halohydrocarbon synthesis by bromoperoxidase. *Science* **1978**, *202*, 1094–1096.

(10) Küpper, F. C.; Schweigert, N.; Gall, E. A.; Legendre, J.-M.; Vilter, H.; Kloareg, B. Iodine uptake in laminariales involves extracellular, haloperoxidase-mediated oxidation of iodide. *Planta* **1998**, *207*, 163–171.

(11) Küpper, F. C.; Carpenter, L. J.; McFiggans, G. B.; Palmer, C. J.; Waite, T. J.; Boneberg, E.-M.; Woitsch, S.; Weiller, M.; Abela, R.; Grolimund, D.; Potin, P.; Butler, A.; Luther, G. W., III; Kroneck, P. M. H.; Meyer-Klaucke, W.; Feiters, M. C. Iodide accumulation provides kelp with an inorganic antioxidant impacting atmospheric chemistry. *Proc. Natl. Acad. Sci. U. S. A.* **2008**, *105*, 6954–6958.

(12) Carpenter, L. J. Iodine in the marine boundary layer. *Chem. Rev.* **2003**, *103*, 4953–4962.

(13) Saiz-Lopez, A.; Plane, J. M. C. Novel iodine chemistry in the marine boundary layer. *Geophys. Res. Lett.* **2004**, *31*, L04112.

(14) Möller, A.; Lovric, M.; Scholz, F. Evidence for the occasional appearance of molecular iodine in sea water. *Int. J. Environ. Anal. Chem.* **1996**, *63*, 99–106.

(15) Garland, J. A.; Curtis, H. Emission of iodine from the sea surface in the presence of ozone. *J. Geophys. Res.: Oceans* **1981**, *86*, 3183–3186.

(16) Carpenter, L. J.; MacDonald, S. M.; Shaw, M. D.; Kumar, R.; Saunders, R. W.; Parthipan, R.; Wilson, J.; Plane, J. M. C. Atmospheric iodine levels influenced by sea surface emissions of inorganic iodine. *Nat. Geosci.* **2013**, *6*, 108–111.

(17) Moore, R. M.; Zafiriou, O. C. Photochemical production of methyl iodide in seawater. *J. Geophys. Res.: Atmos.* **1994**, *99*, 16415–16420.

(18) Martino, M.; Mills, G. P.; Woeltjen, J.; Liss, P. S. A new source of volatile organoiodine compounds in surface seawater. *Geophys. Res. Lett.* **2009**, *36*, L01609.

(19) Takenaka, N.; Ueda, A.; Maeda, Y. Acceleration of the rate of nitrite oxidation by freezing in aqueous solution. *Nature* **1992**, *358*, 736–738.

(20) Takenaka, N.; Ueda, A.; Daimon, T.; Bandow, H.; Dohmaru, T.; Maeda, Y. Acceleration mechanism of chemical reaction by

DOI: 10.1021/acs.est.8b06638
Environ. Sci. Technol. 2019, 53, 4892–4900

freezing: the reaction of nitrous acid with dissolved oxygen. *J. Phys. Chem.* **1996**, *100*, 13874−13884.
(21) Kim, K.; Chung, H. Y.; Ju, J.; Kim, J. Freezing-enhanced reduction of chromate by nitrite. *Sci. Total Environ.* **2017**, *590*−*591*, 107−113.
(22) Min, D. W.; Choi, W. Accelerated reduction of bromate in frozen solution. *Environ. Sci. Technol.* **2017**, *51*, 8368−8375.
(23) Choi, Y.; Yoon, H.-I.; Lee, C.; Vetráková, L'.; Heger, D.; Kim, K.; Kim, J. Activation of periodate by freezing for the degradation of aqueous organic pollutants. *Environ. Sci. Technol.* **2018**, *52*, 5378−5385.
(24) Bartels-Rausch, T.; Jacobi, H.-W.; Kahan, T. F.; Thomas, J. L.; Thomson, E. S.; Abbatt, J. P. D.; Ammann, M.; Blackford, J. R.; Bluhm, H.; Boxe, C.; Domine, F.; Frey, M. M.; Gladich, I.; Guzmán, M. I.; Heger, D.; Huthwelker, Th.; Klán, P.; Kuhs, W. F.; Kuo, M. H.; Maus, S.; Moussa, S. G.; McNeill, V. F.; Newberg, J. T.; Pettersson, J. B. C.; Roeselová, M.; Sodeau, J. R. A review of air-ice chemical and physical interactions (AICI): liquids, quasi-liquids, and solids in snow. *Atmos. Chem. Phys.* **2014**, *14*, 1587−1633.
(25) O'Concubhair, R.; Sodeau, J. R. The effect of freezing on reactions with environmental impact. *Acc. Chem. Res.* **2013**, *46*, 2716−2724.
(26) Takenaka, N.; Bandow, H. Chemical kinetics of reactions in the unfrozen solution of ice. *J. Phys. Chem. A* **2007**, *111*, 8780−8786.
(27) Heger, D.; Jirkovský, J.; Klán, P. Aggregation of methylene blue in frozen aqueous solutions studied by absorption spectroscopy. *J. Phys. Chem. A* **2005**, *109*, 6702−6709.
(28) Heger, D.; Klánová, J.; Klán, P. Enhanced protonation of cresol red in acidic aqueous solutions caused by freezing. *J. Phys. Chem. B* **2006**, *110*, 1277−1287.
(29) O'Driscoll, P.; Lang, K.; Minogue, N.; Sodeau, J. Freezing halide ion solutions and the release of interhalogens to the atmosphere. *J. Phys. Chem. A* **2006**, *110*, 4615−4618.
(30) O'Driscoll, P.; Minogue, N.; Takenaka, N.; Sodeau, J. Release of nitric oxide and iodine to the atmosphere from the freezing of sea-salt aerosol components. *J. Phys. Chem. A* **2008**, *112*, 1677−1682.
(31) O'Sullivan, D.; Sodeau, J. R. Freeze-induced reactions: formation of iodine-bromine interhalogen species from aqueous halide ion solutions. *J. Phys. Chem. A* **2010**, *114*, 12208−12215.
(32) Kim, K.; Yabushita, A.; Okumura, M.; Saiz-Lopez, A.; Cuevas, C. A.; Blaszczak-Boxe, C. S.; Min, D. W.; Yoon, H.-I.; Choi, W. Production of molecular iodine and tri-iodide in the frozen solution of iodide: implication for polar atmosphere. *Environ. Sci. Technol.* **2016**, *50*, 1280−1287.
(33) Raso, A. R. W.; Custard, K. D.; May, N. W.; Tanner, D.; Newburn, M. K.; Walker, L.; Moore, R. J.; Huey, L. G.; Alexander, L.; Shepson, P. B.; Pratt, K. A. Active molecular iodine photochemistry in the Arctic. *Proc. Natl. Acad. Sci. U. S. A.* **2017**, *114*, 10053−10058.
(34) Spolaor, A.; Vallelonga, P.; Plane, J. M. C.; Kehrwald, N.; Gabrieli, J.; Varin, C.; Turetta, C.; Cozzi, G.; Kumar, R.; Boutron, C.; Barbante, C. Halogen species record Antarctic sea ice extent over glacial−interglacial periods. *Atmos. Chem. Phys.* **2013**, *13*, 6623−6635.
(35) Gálvez, Ó.; Baeza-Romero, M. T.; Sanz, M.; Saiz-Lopez, A. Photolysis of frozen iodate salts as a source of active iodine in the polar environment. *Atmos. Chem. Phys.* **2016**, *16*, 12703−12713.
(36) Baker, A. R. Inorganic iodine speciation in tropical atlantic aerosol. *Geophys. Res. Lett.* **2004**, *31*, L23S02.
(37) Elderfield, H.; Truesdale, V. W. On the biophilic nature of iodine in seawater. *Earth Planet. Sci. Lett.* **1980**, *50*, 105−114.
(38) Kieber, R. J.; Rhines, M. F.; Willey, J. D.; Avery, G. B., Jr. Nitrite variability in coastal north carolina rainwater and its impact on the nitrogen cycle in rain. *Environ. Sci. Technol.* **1999**, *33*, 373−377.
(39) Doane, T. A. The abiotic nitrogen cycle. *ACS Earth Space Chem.* **2017**, *1*, 411−421.
(40) Whittaker, M.; Bergmann, D.; Arciero, D.; Hooper, A. B. Electron transfer during the oxidation of ammonia by the chemolithotrophic bacterium *Nitrosomonas europaea*. *Biochim. Biophys. Acta, Bioenerg.* **2000**, *1459*, 346−355.
(41) Carlucci, A. F.; Hartwig, E. O.; Bowes, P. M. Biological production of nitrite in seawater. *Mar. Biol.* **1970**, *7*, 161−166.
(42) Hui, C.; Guo, X.; Sun, P.; Khan, R. A.; Zhang, Q.; Liang, Y.; Zhao, Y.-H. Removal of nitrite from aqueous solution by *Bacillus amyloliquefaciens* biofilm adsorption. *Bioresour. Technol.* **2018**, *248*, 146−152.
(43) Puckett, L. J. Identifying the major sources of nutrient water pollution. *Environ. Sci. Technol.* **1995**, *29*, 408A−414A.
(44) Awtrey, A. D.; Connick, R. E. The absorption spectra of I_2, I_3^-, I^-, IO_3^-, $S_4O_6^=$ and $S_2O_3^=$. heat of the reaction $I_3^- = I_2 + I^-$. *J. Am. Chem. Soc.* **1951**, *73*, 1842−1843.
(45) Vetráková, L'.; Vykoukal, V.; Heger, D. Comparing the acidities of aqueous, frozen, and freeze-dried phosphate buffers: is there a ″pH memory″ effect? *Int. J. Pharm.* **2017**, *530*, 316−325.
(46) Krausková, L'.; Procházková, J.; Klašková, M.; Filipová, L.; Chaloupková, R.; Malý, S.; Damborský, J.; Heger, D. Suppression of protein inactivation during freezing by minimizing pH changes using ionic cryoprotectants. *Int. J. Pharm.* **2016**, *509*, 41−49.
(47) Damschen, D. E.; Martin, L. R. Aqueous aerosol oxidation of nitrous acid by O_2, O_3 and H_2O_2. *Atmos. Environ.* **1983**, *17*, 2005−2011.
(48) Kominami, H.; Gekko, H.; Hashimoto, K. Photocatalytic disproportionation of nitrite to dinitrogen and nitrate in an aqueous suspension of metal-loaded titanium(IV) oxide nanoparticles. *Phys. Chem. Chem. Phys.* **2010**, *12*, 15423−15427.
(49) Lide, D. R. *CRC Handbook of Chemistry and Physics*, 77th, ed.; CRC Press: Boca Raton, FL, 1996.
(50) Sander, R. Compilation of Henry's law constants (version 4.0) for water as solvent. *Atmos. Chem. Phys.* **2015**, *15*, 4399−4981.
(51) Fairbrother, F. Colour of iodine solutions. *Nature* **1947**, *160*, 87.
(52) Sturges, W. T.; Barrie, L. A. Chlorine, bromine and iodine in arctic aerosols. *Atmos. Environ.* **1988**, *22*, 1179−1194.
(53) Oltmans, S. J.; Komhyr, W. D. Surface ozone distributions and variations from 1973−1984: measurements at the NOAA geophysical monitoring for climatic change baseline observatories. *J. Geophys. Res.: Atmos.* **1986**, *91*, 5229−5236.
(54) Rottman, C.; Grader, G.; Hazan, Y. D.; Melchior, S.; Avnir, D. Surfactant-induced modification of dopants reactivity in sol-gel matrixes. *J. Am. Chem. Soc.* **1999**, *121*, 8533−8543.
(55) Perrin, D. D. Buffers of low ionic strength for spectrophotometric p*K* determinations. *Aust. J. Chem.* **1963**, *16*, 572−578.
(56) Dean, J. A. *Lange's Handbook of Chemistry*, 14th, ed.; McGraw-Hill: New York, 1992.
(57) Perrin, D. D. *Dissociation Constants of Inorganic Acids and Bases in Aqueous Solutions*; Butterworths: London, 1969.
(58) Riordan, E.; Minogue, N.; Healy, D.; O'Driscoll, P.; Sodeau, J. R. Spectroscopic and optimization modeling study of nitrous acid in aqueous solution. *J. Phys. Chem. A* **2005**, *109*, 779−786.
(59) Smith, D.; Wang, T.; Španěl, P. A SIFT study of the reactions of H_2ONO^+ ions with several types of organic molecules. *Int. J. Mass Spectrom.* **2003**, *230*, 1−9.
(60) Turney, T. A.; Wright, G. A. Nitrous acid and nitrosation. *Chem. Rev.* **1959**, *59*, 497−513.
(61) Durig, J. R.; Bonner, O. D.; Breazealel, W. H. Raman studies of iodic acid and sodium iodate. *J. Phys. Chem.* **1965**, *69*, 3886−3892.
(62) Kim, K.; Kim, J.; Bokare, A. D.; Choi, W.; Yoon, H.-I.; Kim, J. Enhanced removal of hexavalent chromium in the presence of H_2O_2 in frozen aqueous solutions. *Environ. Sci. Technol.* **2015**, *49*, 10937−10944.
(63) Kim, K.; Choi, W. Enhanced redox conversion of chromate and arsenite in ice. *Environ. Sci. Technol.* **2011**, *45*, 2202−2208.
(64) Takenaka, N.; Tanaka, M.; Okitsu, K.; Bandow, H. Rise in the pH of an unfrozen solution in ice due to the presence of NaCl and promotion of decomposition of gallic acids owing to a change in the pH. *J. Phys. Chem. A* **2006**, *110*, 10628−10632.
(65) Jacobi, H.-W.; Kleffmann, J.; Villena, G.; Wiesen, P.; King, M.; France, J.; Anastasio, C.; Staebler, R. Role of nitrite in the

DOI: 10.1021/acs.est.8b06638
Environ. Sci. Technol. 2019, 53, 4892−4900

photochemical formation of radicals in the snow. *Environ. Sci. Technol.* **2014**, *48*, 165−172.
(66) Amoroso, A.; Domine, F.; Esposito, G.; Morin, S.; Savarino, J.; Nardino, M.; Montagnoli, M.; Bonneville, J.-M.; Clement, J.-C.; Ianniello, A.; Beine, H. J. Microorganisms in dry polar snow are involved in the exchanges of reactive nitrogen species with the atmosphere. *Environ. Sci. Technol.* **2010**, *44*, 714−719.
(67) Ito, K.; Takayama, Y.; Makabe, N.; Mitsui, R.; Hirokawa, T. Ion chromatography for determination of nitrite and nitrate in seawater using monolithic ODS columns. *J. Chromatogr. A* **2005**, *1083*, 63−67.
(68) Johnson, K. S.; Petty, R. L. Determination of nitrate and nitrite in seawater by flow injection analysis. *Limnol. Oceanogr.* **1983**, *28*, 1260−1266.
(69) Huang, J.; Liu, P.-r.; Sun, Q.-y.; Zhang, H.; Zhang, Y.; Wang, K. Determination of total nitrogen, ammonia, and nitrite in river water by near-infrared spectroscopy and chemometrics. *Anal. Lett.* **2017**, *50*, 1620−1629.
(70) Zieliński, R.; Dunalska, J.; Grochowska, J.; Bigaj, I.; Szymański, D. Variation of nitrogen forms in lakes with different intensity of anthropogenic pressure. *Limnol. Rev.* **2013**, *13*, 181−188.
(71) Atkinson, H. M.; Huang, R.-J.; Chance, R.; Roscoe, H. K.; Hughes, C.; Davison, B.; Schönhardt, A.; Mahajan, A. S.; Saiz-Lopez, A.; Hoffmann, T.; Liss, P. S. Iodine emissions from the sea ice of the Weddell Sea. *Atmos. Chem. Phys.* **2012**, *12*, 11229−11244.
(72) Schnepfe, M. M. Determination of total iodine and iodate in sea water and in various evaporites. *Anal. Chim. Acta* **1972**, *58*, 83−89.
(73) Yokota, K.; Fukushi, K.; Takeda, S.; Wakida, S.-I. Simultaneous determination of iodide and iodate in seawater by transient isotachophoresis-capillary zone electrophoresis with artificial seawater as the background electrolyte. *J. Chromatogr. A* **2004**, *1035*, 145−150.
(74) Huang, Z.; Ito, K.; Timerbaev, A. R.; Hirokawa, T. Speciation studies by capillary electrophoresis - simultaneous determination of iodide and iodate in seawater. *Anal. Bioanal. Chem.* **2004**, *378*, 1836−1841.
(75) Zhang, S.; Schwehr, K. A.; Ho, Y.-F.; Xu, C.; Roberts, K. A.; Kaplan, D. I.; Brinkmeyer, R.; Yeager, C. M.; Santschi, P. H. A novel approach for the simultaneous determination of iodide, iodate and organo-iodide for ^{127}I and ^{129}I in environmental samples using gas chromatography-mass spectrometry. *Environ. Sci. Technol.* **2010**, *44*, 9042−9048.
(76) Žic, V.; Branica, M. The distributions of iodate and iodide in Rogoznica Lake (East Adriatic Coast). *Estuarine, Coastal Shelf Sci.* **2006**, *66*, 55−66.
(77) Ali, K.; Sonbawane, S.; Chate, D. M.; Siingh, D.; Rao, P. S. P.; Safai, P. D.; Budhavant, K. B. Chemistry of snow and lake water in Antarctic region. *J. Earth Syst. Sci.* **2010**, *119*, 753−762.
(78) Caritat, P. d.; Hall, G.; Gìslason, S.; Belsey, W.; Braun, M.; Goloubeva, N. I.; Olsen, H. K.; Scheie, J. O.; Vaive, J. E. Chemical composition of arctic snow: concentration levels and regional distribution of major elements. *Sci. Total Environ.* **2005**, *336*, 183−199.
(79) Cuevas, C. A.; Maffezzoli, N.; Corella, J. P.; Spolaor, A.; Vallelonga, P.; Kjær, H. A.; Simonsen, M.; Winstrup, M.; Vinther, B.; Horvat, C.; Fernandez, R. P.; Kinnison, D.; Lamarque, J.-F.; Barbante, C.; Saiz-Lopez, A. Rapid increase in atmospheric iodine levels in the north atlantic since the mid-20th century. *Nat. Commun.* **2018**, *9*, 1452.
(80) Saiz-Lopez, A.; Blaszczak-Boxe, C. S.; Carpenter, L. J. A mechanism for biologically induced iodine emissions from sea ice. *Atmos. Chem. Phys.* **2015**, *15*, 9731−9746.

DOI: 10.1021/acs.est.8b06638
Environ. Sci. Technol. 2019, 53, 4892−4900